Research Square

Preprints are preliminary reports that have not undergone peer review.
They should not be considered conclusive, used to inform clinical practice,
or referenced by the media as validated information.

Effects of the cancellous bone structure in the skull on ultrasonic wave propagation

Itsuki Michimoto
Doshisha University
Keita Yano
Doshisha University
Yasuyo Kobayashi
Nara Medical University
Kozue Saito
Nara Medical University
Mami Matsukawa (mmatsuka@mail.doshisha.ac.jp)
Doshisha University

Research Article

Keywords: Transcranial Doppler, Cerebral Blood Flow Velocity, Emboli, Ultrasound Penetration, Temporal Bone Structure, Finite-Difference Time-Domain

Posted Date: December 15th, 2020

DOI: https://doi.org/10.21203/rs.3.rs-124985/v1

License: This work is licensed under a Creative Commons Attribution 4.0 International License.
Read Full License

Abstract

The Transcranial Doppler method (TCD) enables the measurement of cerebral blood flow velocity and detection of emboli by applying the ultrasound probe to the temporal bone window, orbital, or greater occipital foramen. TCD is widely used for the evaluation of cerebral vasospasm after subarachnoid hemorrhage, early detection of patients with arterial stenosis and the check of brain death. However, measurements often become difficult in elderly women. Among various factors for this problem, we focused on the effect of the skull bone on the ultrasound penetration into the brain. Especially, the effect of the temporal bone structure was investigated. Using a 2D digital bone model, wave propagation through the skull bone was investigated by the Finite-Difference Time-Domain (FDTD) method. We create bone models which have different BV/TV (Bone Volume/Total Volume) in diploe. Around BV/TV about 60% (similar to elderly women), the observed maximum amplitude decrease due to multiple reflection and scattering. The results suggest that effects of osteoposis on the skull make TCD measurement difficult.

Introduction

The vertebrate skull has a relatively complicated structure; it mainly consists of the following three layers: the outer (cortical bone), diploe (cancellous bone), and inner (cortical bone) layers. The heterogeneous and anisotropic characteristics of these layers facilitate complex ultrasound propagation; however, recent advances in transcranial ultrasound transmission have provided new noninvasive therapeutic and diagnostic techniques for brain diseases [1,2].

However, most ultrasonic studies have assumed isotropic plate models, which do not accurately represent the actual structural and material characteristics of the skull [3]. Eguchi et al. reported that low-intensity pulsed ultrasound therapy improves cognitive impairment in mouse models of Alzheimer's disease and vascular dementia [4]. For the precise irradiation of ultrasound to the affected part, it is important to control ultrasound radiation, considering the complicated characteristics of skull.

Among many diagnostic techniques for brain diseases, the transcranial Doppler (TCD) method is an approach that involves the application of an ultrasonic probe to the temporal bone window or the orbital or greater occipital foramen to evaluate cerebral blood flow velocity and detect emboli. It was first reported by Aaslid et al. in 1982 [5]. Since then, the TCD method has been widely used in clinical practices for the evaluation of cerebral vasospasms after subarachnoid hemorrhage, early detection of thrombus in patients with arterial stenosis or left ventricular assistive heart [6], and determination of brain death [7]. However, it has recently been reported that measurements often become difficult in elderly Japanese women [8]. One possible reason may be the morphological changes in the skull that accompany aging. Kaito reported that the thickness of the skull increases in the elderly [9]. In addition, primary and secondary osteoporosis may affect ultrasonic wave propagation. It is a well-known fact that the bone volume fraction in the cancellous bone decreases with the progression of osteoporosis [10]. Excessive decrease in bone volume fraction may result in strong ultrasound scattering and considerable attenuation

of weak signals of the observed ultrasonic waves. There has been no discussion in the literature on how osteoporosis affects the TCD method.

In this study, we focused on the effects of the cancellous structure on ultrasonic wave propagation by analyzing the propagation phenomenon in a human skull model. Considering bone structural changes due to age, 2D digital partial skull models were created. Finite-difference time-domain (FDTD) simulation was applied to the digital models to assess ultrasonic wave propagation in the thickness direction, which is commonly used with the TCD method.

Model And Method

2D digital temporal bone model

In this study, four types of models were fabricated and are shown in Figure 2. In the first model (empty model), the diploe was filled with water to mimic bone marrow (BV/TV = 0%). In the second model (uniform model), the diploe was filled with bone (BV/TV = 100%). In the third model (sample A), the trabecular bone was aligned nearly parallel to the cortical bone layer, and the diploe was filled with water and the trabecular bone was created from a CT image of the actual cancellous bone in an equine femur. The trabeculae were highly aligned and showed a high degree of anisotropy (DA; 2.5). In the fourth model (sample B), the trabeculae were mostly aligned perpendicular to the cortical layer. This was created from a CT image of the cancellous bone of a swine skull. Figure 2 shows examples with the BV/TV of bone (50%–60%) that was similar to the BV/TV of an elderly human skull [12]. Because the CT images are shown using grayscale (0–255), the models were created by choosing several different grayscale thresholds to change BV/TV. However, control of the grayscale did not have a strong influence on the alignment direction of the trabeculae. Here in the case of sample A, 15 thresholds in a 256-scale gray image were selected. The BV/TV values of the models from sample A are shown in Table 1 (a). In the case of sample B, 11 thresholds were selected. The BV/TV of the models are shown in Table 1 (b).

FDTD method

An elastic 2D FDTD simulation was performed to simulate the longitudinal and shear wave propagation in the model [13,14]. Similar to the previous studies by our group [15,16], an in-house FDTD source code was used. This simulation did not consider attenuation during propagation. The relevant equations for the x direction are Eqs. (1)–(3):

$$\frac{\partial \sigma_{xx}}{\partial t} = c_{11}\frac{\partial v_x}{\partial x} + c_{12}\frac{\partial v_y}{\partial y}, \quad (1)$$

$$\frac{\partial \sigma_{xy}}{\partial t} = \frac{\partial \sigma_{yx}}{\partial t} = c_{44}\left(\frac{\partial v_x}{\partial y} + \frac{\partial v_y}{\partial x}\right), \quad (2)$$

$$\frac{\partial v_x}{\partial t} = \frac{1}{\rho}\left(\frac{\partial \sigma_{xx}}{\partial x} + \frac{\partial \sigma_{xy}}{\partial y}\right), \quad (3)$$

whereσ_{xx}, σ_{xy}, v, and ρ represent the normal stress, shear stress, particle velocity, and density of the medium, respectively. Next, we estimated the associated elastic constants. The matrix of elastic constants is shown in Eq. (4):

$$c = \begin{pmatrix} c_{11} & c_{12} & 0 & 0 \\ c_{21} & c_{11} & 0 & 0 \\ 0 & 0 & c_{44} & 0 \\ 0 & 0 & 0 & c_{44} \end{pmatrix}, \quad (4)$$

Here, direction 1 is the front–back direction of the skull and direction 2 is the thickness direction. The constants of the model were assumed to be homogeneous. c11 was estimated from the speed of sound in the axial direction of the bovine femur cortical bone, referring to a study by Yamato et al. c44 was obtained assuming the Poisson's ratio of 0.33 [17-19].

These equations were calculated digitally using the central difference method. The stress and particle velocity were both calculated alternately in the spatial and time domains, which is called "the leapfrog method." The Higdon's second-order absorption boundary condition was implemented at the edges of the simulation area as an absorption layer [20].

Method (Condition)

Figure 3 shows the simulation model that was used. A transmitter array (length = 20 mm) was placed outside the bone model and in front of the thinnest part of the bone. The transmitter was an array of 100 transducers that controlled the phase to focus the wave near the artery. The bone model was placed 2 mm from the transmitter after considering skin thickness. The receiver array (length of each receiver was 1 mm) was placed 60 mm from the transmitter. The receiver and artery positions were similar to the expected positions of middle cerebral artery or posterior cerebral artery, which are usually measured from the temporal bone window by TCD [21]. The position of the artery is expected to be at the center of the receivers. The radiated waveform from the transmitter was a single sinusoidal wave at 2 MHz with a Hann window.

The spatial and time resolutions in the simulations were 14 μm and 2.5 ns, respectively. These resolutions satisfied the Courant stability condition [22]. In this simulation, the model was immersed in water to mimic the surrounding soft tissues. The longitudinal wave velocity and density of water were 1500 m/s and 1000 kg/m^3, respectively.

Results And Discussion

Figure 4 (a) shows the observed waves that propagated in water only, i.e., without the bone model. The arrival time of each wavefront was defined at 5% of the maximum amplitude of the first positive peak. The highest amplitude was observed at the center of the receiver array (x = 0). Furthermore, as seen in the figure, the observed waveforms showed axis-symmetrical characteristics. The amplitudes decreased with the increase in the distance from the center. The arrival times at x = ±10 were the shortest because the wave that radiated from each end of the transmitter array reached these positions first.

Figure 4 (b) and (c) shows the observed waves that propagated through the empty model and the uniform model, respectively. In the empty model, the wave was focused mostly near the artery (x = 0); however, the maximum amplitude was observed at x = −2 in the uniform model, showing a small shift. Additionally, the waveforms were not axis-symmetric, and the time of the maximum amplitude observation was delayed. This indicated that ultrasound focusing was clearly affected by the complex bone shape.

Sample A

Figure 5 (a) and (b) shows examples of the observed waves that had propagated in sample A (BV/TV = 59% and 49%, respectively). Compared with the waves propagating in water only, the amplitudes were decreased and the arrival time of the wavefronts changed in this sample. Changes in the observed waves could be attributed to the BV/TV. Additionally, small maximum amplitudes were not observed near the wavefronts; they were delayed, similar to the waves of the uniform model. Figure 5 (c) shows the relationship between BV/TV and the maximum amplitude observed at the receiver array. The maximum amplitude decreased rapidly at a BV/TV of approximately 50% and subsequently fluctuated due to the increase in BV/TV. The maximum amplitudes increased at a BV/TV of >70%. There was a wide area with large amplitudes. However, the positions of the receiver that showed the maximum amplitudes were not centered (x = 0) and were shifted to a slight extent at a BV/TV of 55%–65%.

Sample B

Figure 6 (a) shows the observed waves that had propagated in sample B (BV/TV = 49%). Similarly, the arrival time of the wavefronts had changed in sample B. Figure 6 (b) shows the relationship between

BV/TV and the maximum amplitude observed at the receiver array. Around a BV/TV of 55%, the maximum amplitude showed the minimum value. At a BV/TV of 50%–55%, the positions of the receivers that showed the maximum amplitudes shifted by approximately 10 mm in the direction of the x-axis from the center (x = 0).

Discussion

In this study, the maximum amplitudes changed due to the BV/TV in samples A and B. Larsson et al. reported a decrease in BV/TV in cancellous bones with age [12]. They showed that BV/TV in the skull bone of a 70-year-old woman was approximately 62%, whereas that of a 50-year-old woman was approximately 82%. These results indicate that decreasing BV/TV with age may prevent ultrasounds from reaching the arteries. This may make it difficult to obtain TCD measurements in elderly women. In the skull, the main alignment of the trabeculae is considered to be in the direction of the thickness [23]. Therefore, the condition might be similar to that found in sample B. In case of sample B, there was a clear decrease in the maximum amplitude at a BV/TV of approximately 50%–55%, which are similar to the values reported in elderly patients.

The observed wave can be analyzed to easily reveal that the waves accompanied several small waves after passing through the bone. The small waves may originate from the multiple reflections and scattering. Subsequently, we checked the effects of scattering and reflections from the observed waveforms. Notably, as opposed to the waves that passed through water only, several late small waves were observed in the data of samples A and B. In addition, increase in back scattering and scattering in the other directions may result in a decrease in the total energy of the observed waves. Figure 7 shows the relationship between the sum of the squared signals [p^2 shown in Eq. (5)] observed at each receiver and BV/TV in sample B.

$$p^2 = \int_0^T (\sigma_{xx}(t))^2 \, dt \qquad (5)$$

Here, the observation time T was 50.5 μs. The horizontal axis shows the position of observing the array transducer and the vertical axis shows the BV/TV of the bone sample. At a BV/TV of approximately 55%, there is a decrease in the values of p^2. This implies that the energy passing through the bone decreases due to scattering and multiple reflections.

In sample B, there was a minor shift in the maximum amplitude position to the positive direction of *x*. This could be attributed to the slight counterclockwise tilted in the trabeculae from the thickness. Consequently, ultrasound may be refracted in the bone model. Yamashita et. al. reported that the bone trabecular alignment affected the direction of ultrasound propagation [24]. In this model, the bone trabecular alignment tilted to the positive direction of x. The ultrasound subsequently did not focus

strongly near the artery, and the maximum amplitude positions shifted. Similar scattering phenomena and refraction of the waves may occur in an actual skull bone.

Conclusion

In this study, the effect of skull bone structural changes on ultrasound propagation was investigated by FDTD simulation. By changing the trabecular BV/TV in the 2D human temporal bone models, we found a decrease in ultrasound amplitudes owing to the presence of scattering and reflections. Ultrasound attenuated well in the bone with a BV/TV of 60%, which was similar to the BV/TV value of the diploe in the skull of elderly women. The structural changes in the skull may affect ultrasonic penetration into the brain and may be one factor that can explain the difficulty in measuring TCD in elderly Japanese women. This study also indicates that the effect of skull structure on the ultrasound propagation is also an important factor for future brain therapy and diagnosis.

Declarations

Acknowledgments

We thank Japan Science and Technology Agency and Japan Keirin Association for supporting part of this study.

Author contributions

I. M., K. Y., and M. M. contributed to the study concept and its design. I. M., K. Y., and M. M. contributed to data acquisition. I. M., K. Y., and M. M. contributed to analyses. I. M., Y. K., K. S., and M. M. contributed to data interpretation. All author read and approved the final manuscript.

Declaration of competing interest

The authors declare no competing interests.

References

1. Krishna, F. Sammartino, A. Rezai, “A review of the current therapies, challenges and future directions of transcranial focused ultrasound technology”, JAMA Neurol. **75**, 246-254 (2018).
2. Ghanouni, et al., “Transcranial MRI-guided focused ultrasound: A review of the technologic and neurologic applications”, Am. J. Roentgenology, **205**, 150-159 (2015).
3. Sun, K. Hynynen, “Focusing of the rapeutic ultrasound through a human skull: A numerical study”, The Journal of the Acoustical Society of America, **104**, 1705-1715 (1998)

4. Eguchi, et al., “Whole-brain low-intensity pulsed ultrasound therapy markedly improves cognitive dysfunctions in mouse models of dementia – Crucial roles of endothelial nitric oxide synthase”, **11**, 959-973 (2018).
5. Aaslid, T. M. Markwalder, H. Nornes, “Noninvasive transcranial Doppler ultrasound recording of flow velocity in basal cerebral arteries”, J Neurosurg, **57**, 769-774 (1982).
6. Seguchi, et al., “Evaluation of micro-emboli in a patient with ventricular assist device support with hemolysis.”, J Artif Organs., **18**, 276-279 (2015).
7. Lampl Y, et al., “Diagnosing brain death using the transcranial Doppler with a transorbital approach”, Arch Neurol., **59**, 58-60 (2002).
8. Hashimoto, H. Etani, M. Naka, N. Kinoshita, T. Nukada, “Assessment of the rate of successful Transcranial Doppler recording through the temporal windows in Japanese with .special reference to aging and sex”, Japanese Journal of Geriatrics, **29**, 119-122 (1992)
9. Kaito, “On the thickness of the Japanese skull”, Tokyo Jikeikai medical journal, **95**, 503-513 (1980).
10. Inaba, et al., “Preferential reductions of paraarticular trabecular bone component in ultradistal radius and of calcaneus ultrasonogaraphy in early-stage rheumatoid arthritis”, Osteoporosis Int., **14**, 683-687 (2003).
11. 3DCG head data base developed by Department of Neurosurgery, The University of Tokyo, https://brain-3dcg.org/.
12. Larsson, et al., “Morphological characterization of the human calavarium in relation to the diploic and cranial thickness utilizing x-ray computed microtomography”, IFMBE Proceedings, **41**, 194-197 (2013).
13. Yee, “Numerical solution of initial boundary value problems inVolving Maxwell’s equations in isotropic media,” IEEE Trans. Antenna Propag., **14**, 302–307 (1966).
14. F. Toro, J. F. Clarke, “Numerical Methods for Wave Propagation”, (Kluwer Academic Pub., 1998).
15. Nagatani, et al., “Applicability of Finite-Difference Time-Domain Method to simulation of wave propagation in cancellous bone”, Jpn. J. Appl. Phys., **45**, 71-86 (2006).
16. Nagatani, et al., “Propagation of fast and slow waves in cancellous bone; Comparative study of simulation and experiment”, Acoust. Sci. Technol., **30**, 257-264 (2009).
17. L. Rose, “Ultrasonic Waves in Solid Media”, 367 (Cambridge University Press, Cambridge, U.K., 1999).
18. H. Smit, J.M. Huyghe, S.C. Cowin, “Estimation of the poroelastic parameters of cortical bone”, J. Biomech., **35**, 829-835 (2002).
19. Hosokawa, T. Otani, “Ultrasonic wave propagation in bovine cancellous bone”, J. Acoust. Soc. Am., **101**, 558 (1997).
20. L. Higdon, “Absorbing boundary conditions for difference approximations to the multidimensional wave equation”, Math. Comput., **47**, 437-459 (1986).
21. Nakane, C. Nemoto, H. Maru, M. Murakawa, “Clinical monitoring of cerebral blood flow velocity with transcranial Doppler sonography”, The Journal of Japan Society for Clinical Anesthesia, **25** (2005).

22. Courant, K. Friedrichs, H. Lewy, “On the Partial Difference Equations of Mathematical Physics”, IBM J. RES. Develop., **11**, 215-234 (1967).
23. Pinton, et al., “Attenuation, scattering, and absorption of ultrasound in the skull bone”, Medical Physics, **39**, 299-307 (2012).
24. Yamashita, F. Fujita. K. Mizuno, I. Mano, M. Matsaukawa, “Two-wave propagation imaging to evaluate the structure of cancellous bone”, IEEE Trans Ulrason Ferroelectr Frew Control., **59**, (2012).

Tables

Table 1 BV/TV of bone models

Sample A		Sample B	
Threshold	BV/TV [%]	Threshold	BV/TV [%]
60	74	95	67
70	70	100	65
88	67	105	63
95	66	110	60
110	64	115	58
130	61	120	55
140	60	125	52
150	59	130	49
160	57	132	48
170	55	135	46
180	53		
185	51		
190	49		
192	47		

Figures

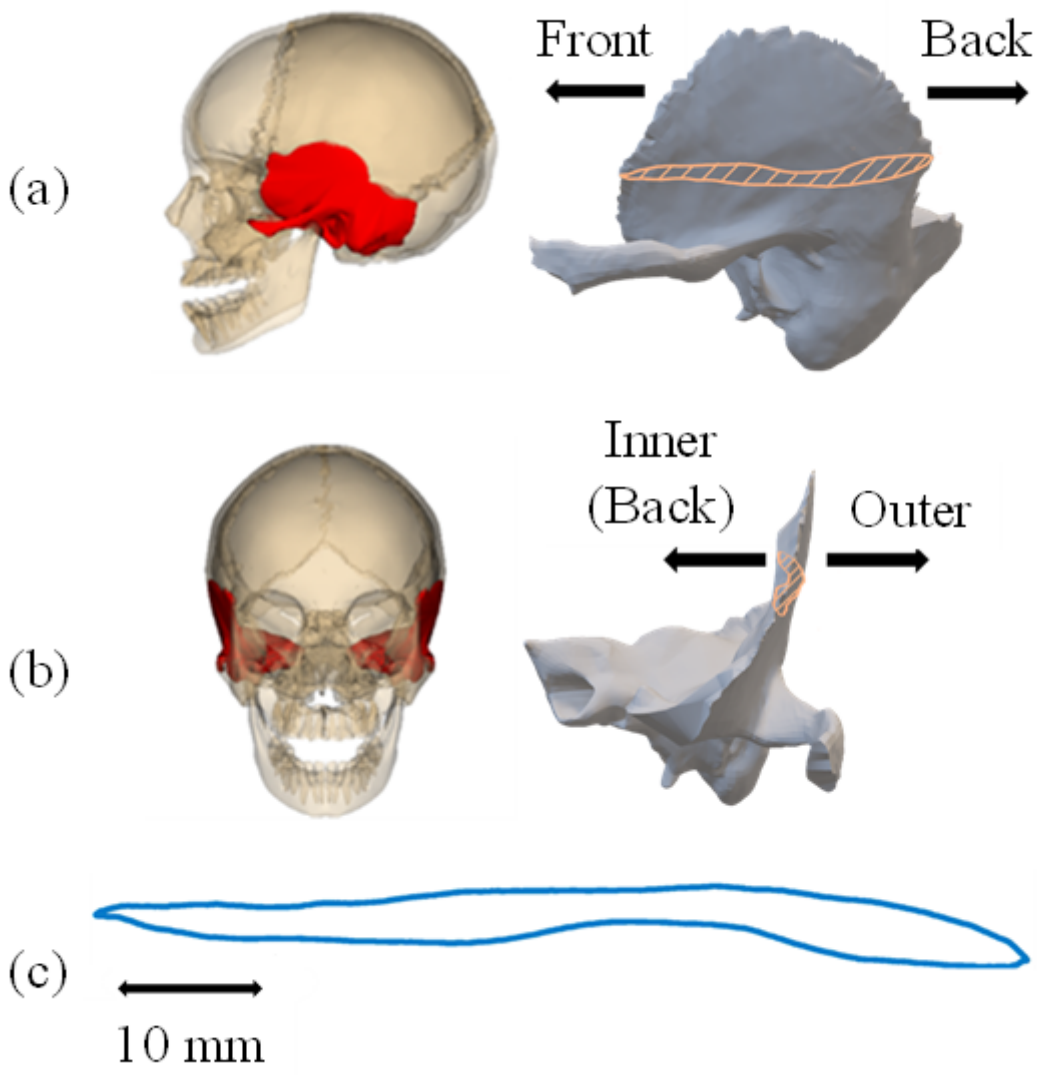

Figure 1

A cross-section view of the thinnest part of left temporal bone.

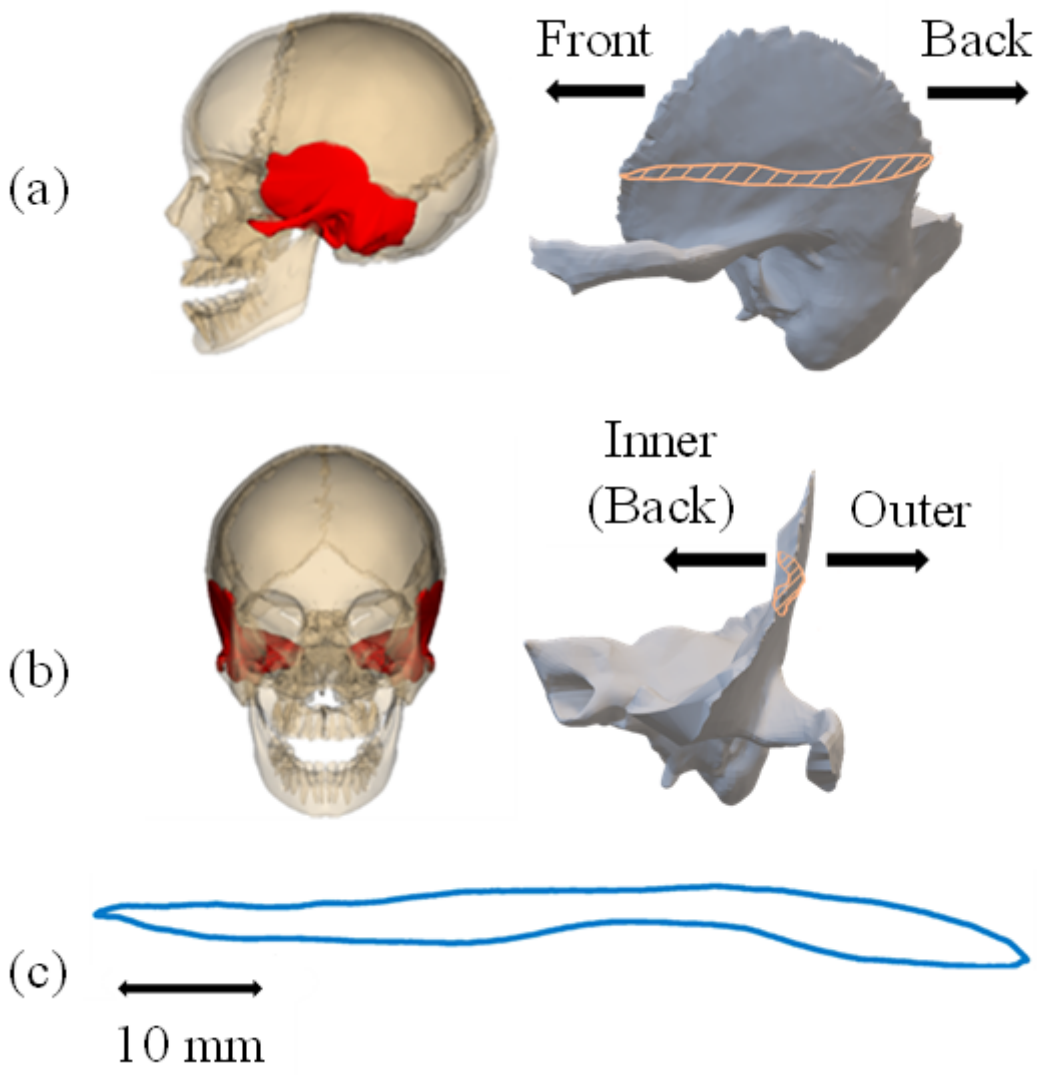

Figure 1

A cross-section view of the thinnest part of left temporal bone.

Figure 2

Four bone models (a) empty model (b) uniform model (c) parallel model (59 %) (d) vertical model (55 %)

Figure 2

Four bone models (a) empty model (b) uniform model (c) parallel model (59 %) (d) vertical model (55 %)

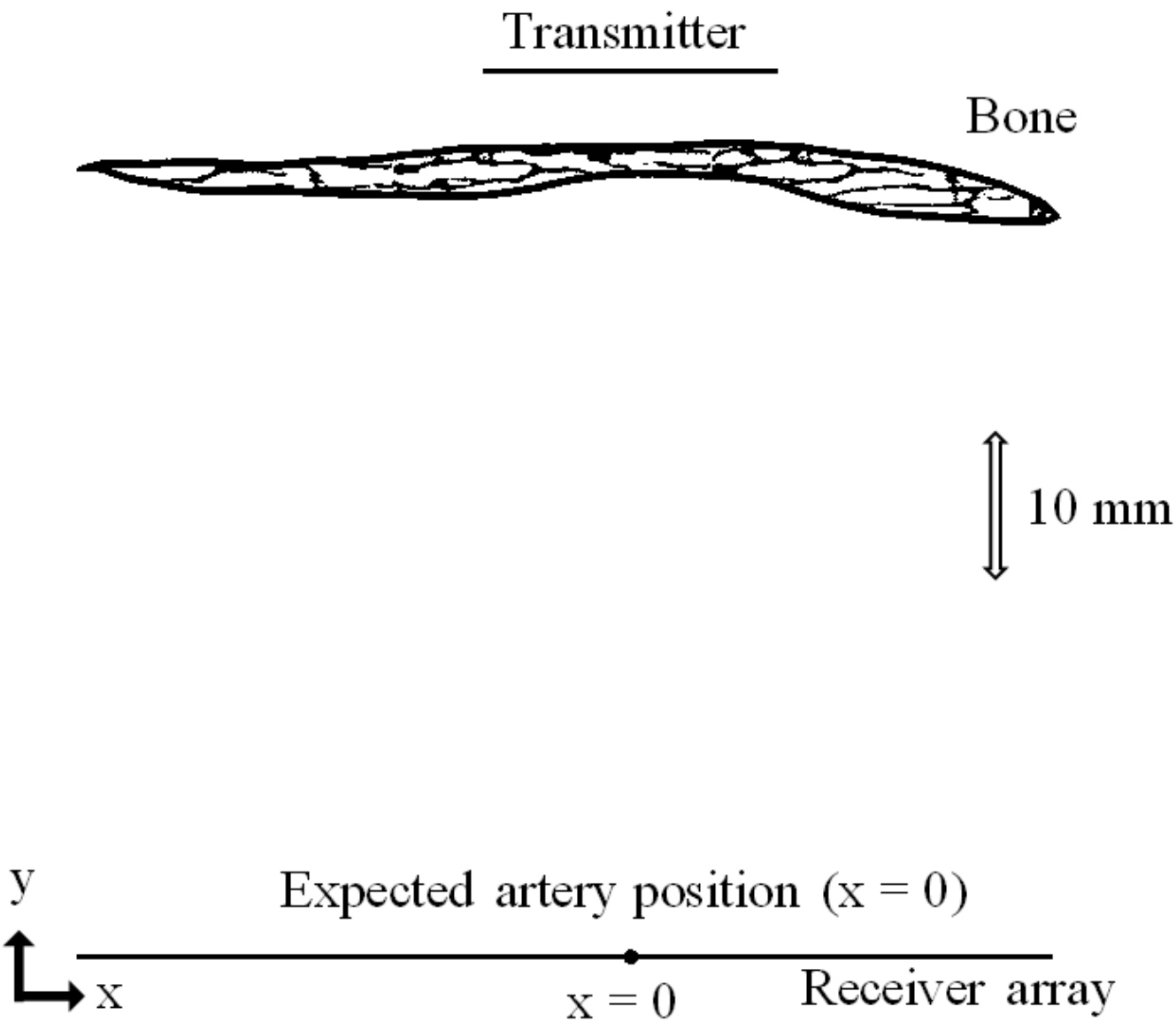

Figure 3

Simulation conditions. The center positions of the transmitter and receiver arrays are at x = 0. The transmitter and receiver arrays are set parallel with distance of 60 mm.

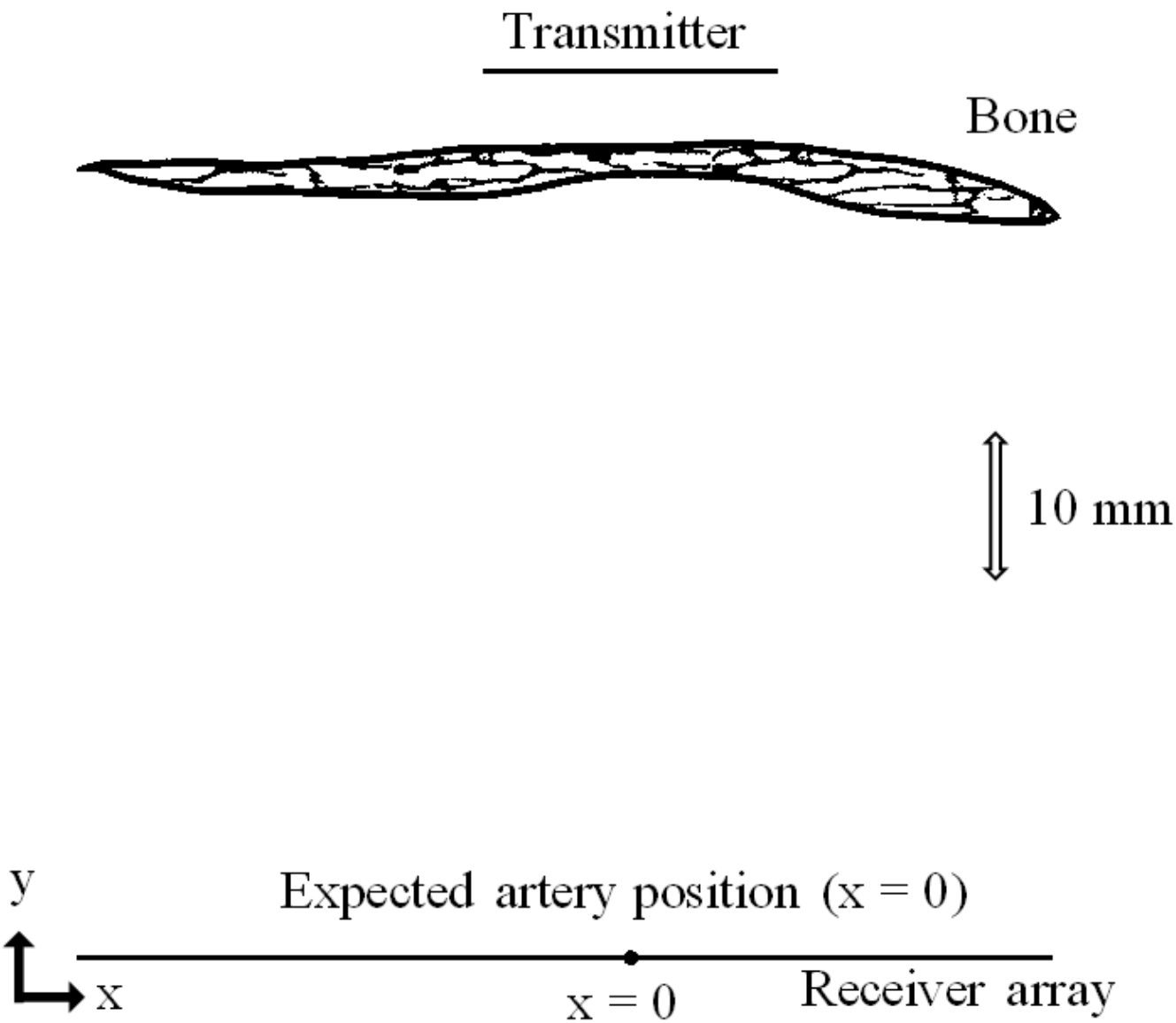

Figure 3

Simulation conditions. The center positions of the transmitter and receiver arrays are at x = 0. The transmitter and receiver arrays are set parallel with distance of 60 mm.

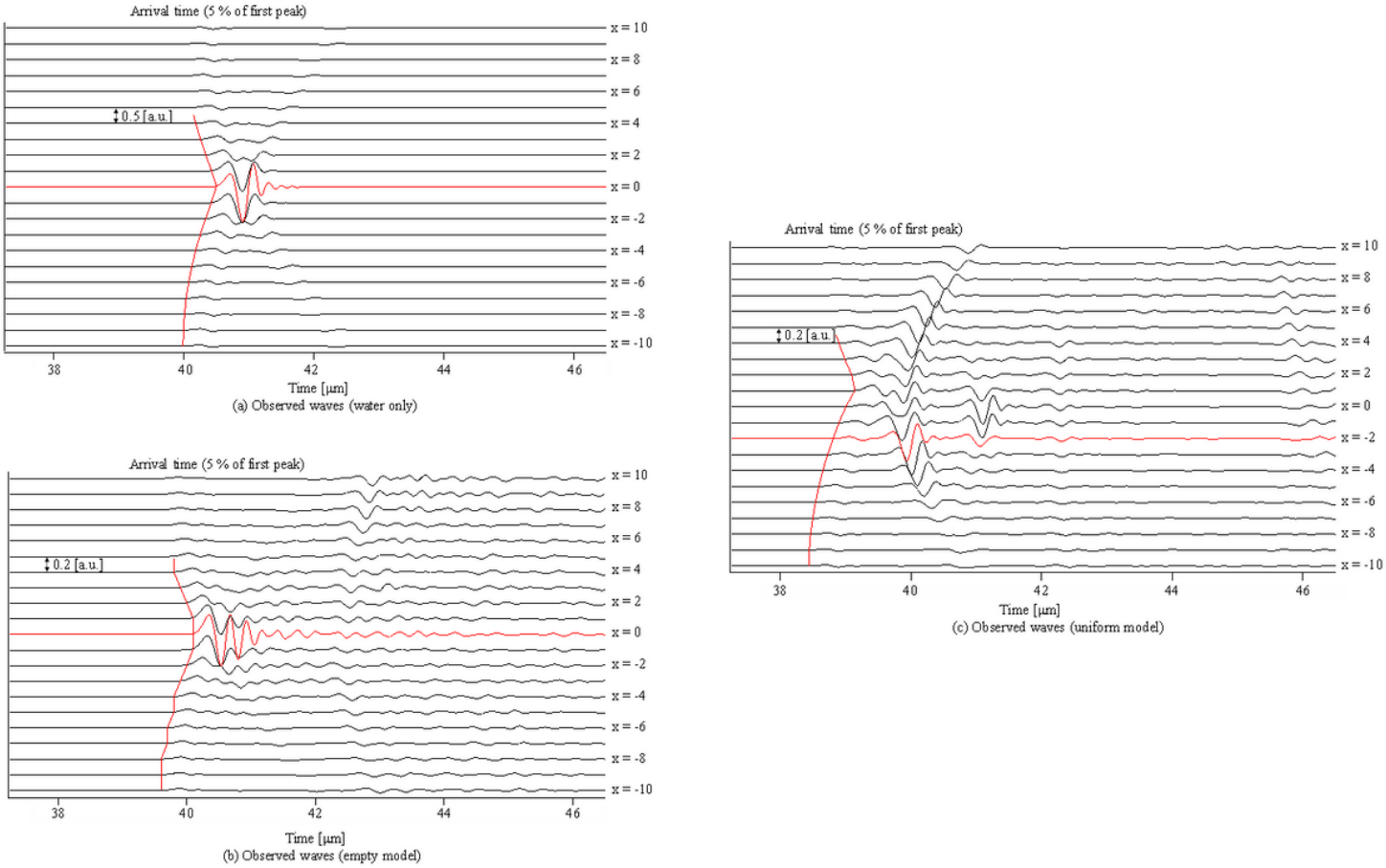

Figure 4

(a) Observed waves (water only) at the receiver array near the center. (b) Observed waves (empty model: BV/TV = 0 %) at the receiver array near the center. (c) Observed waves (uniform model: BV/TV 100 %) at the receiver array near the center.

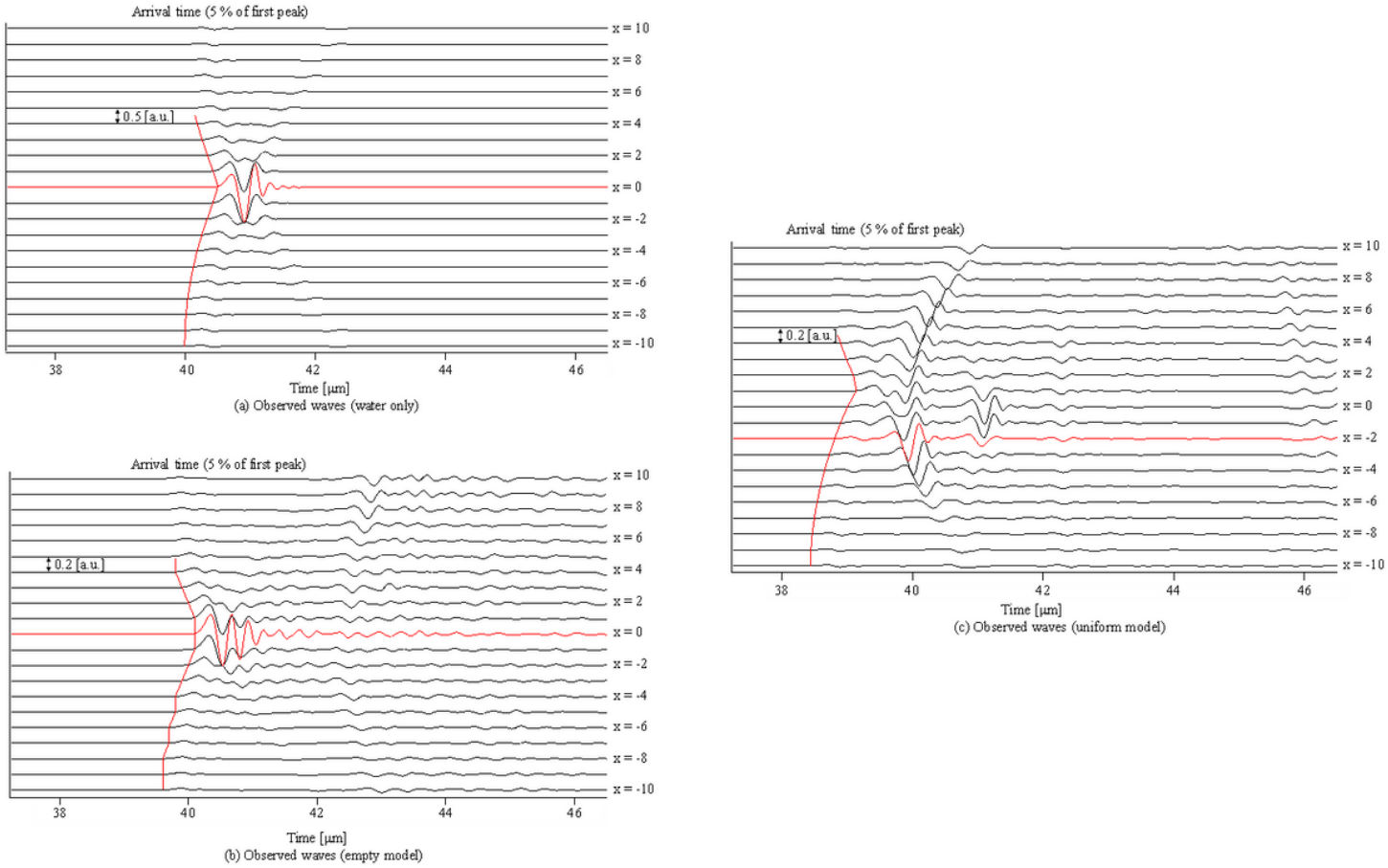

Figure 4

(a) Observed waves (water only) at the receiver array near the center. (b) Observed waves (empty model: BV/TV = 0 %) at the receiver array near the center. (c) Observed waves (uniform model: BV/TV 100 %) at the receiver array near the center.

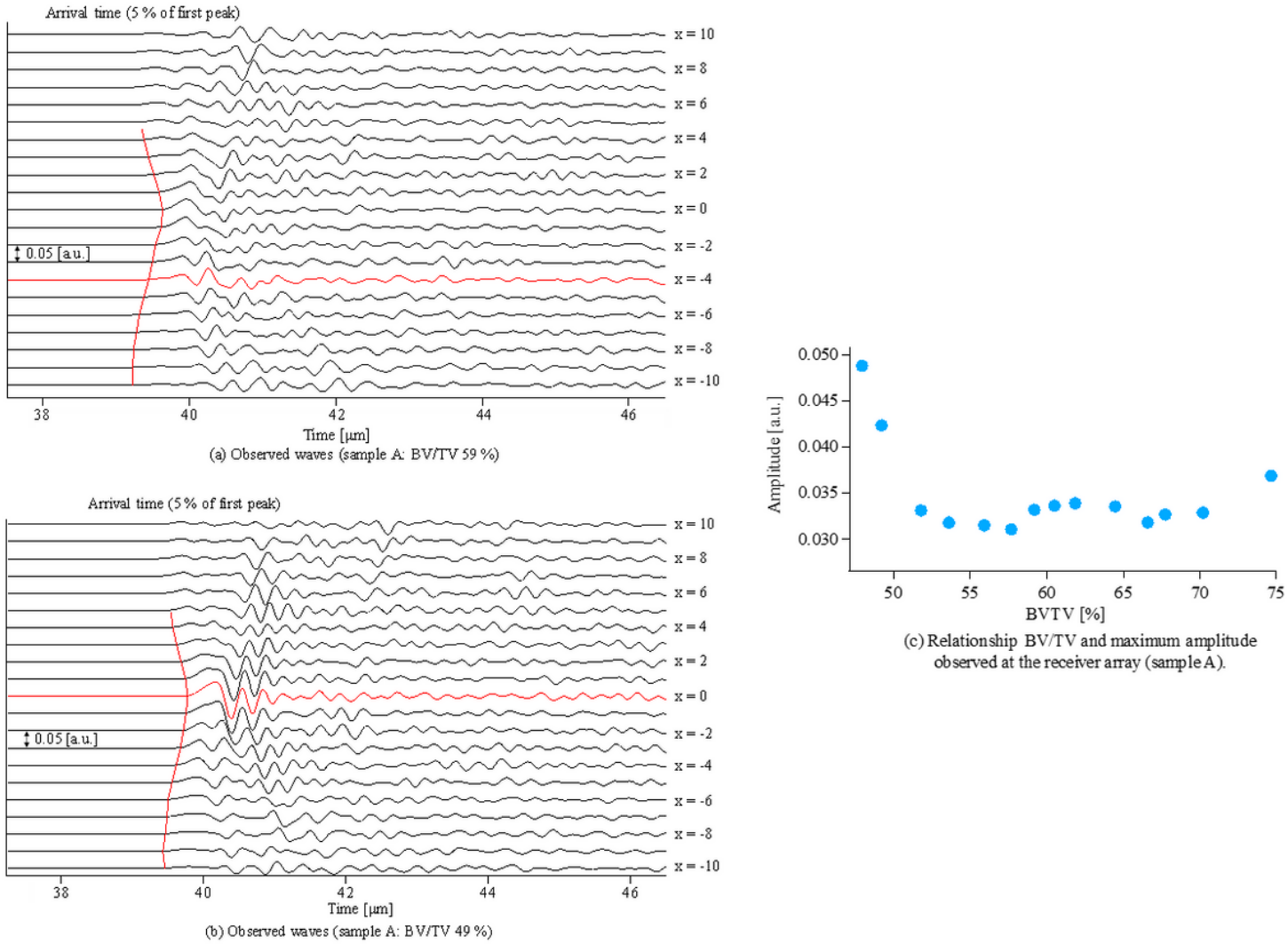

Figure 5

(a) Observed waves which passed through the sample A (BV/TV 59 %), near the center of the receiver array. (b) Observed waves which passed through the sample A (BV/TV 49 %), near the center of the receiver array. (c) Relationship BV/TV and maximum amplitude observed at the receiver array (sample A).

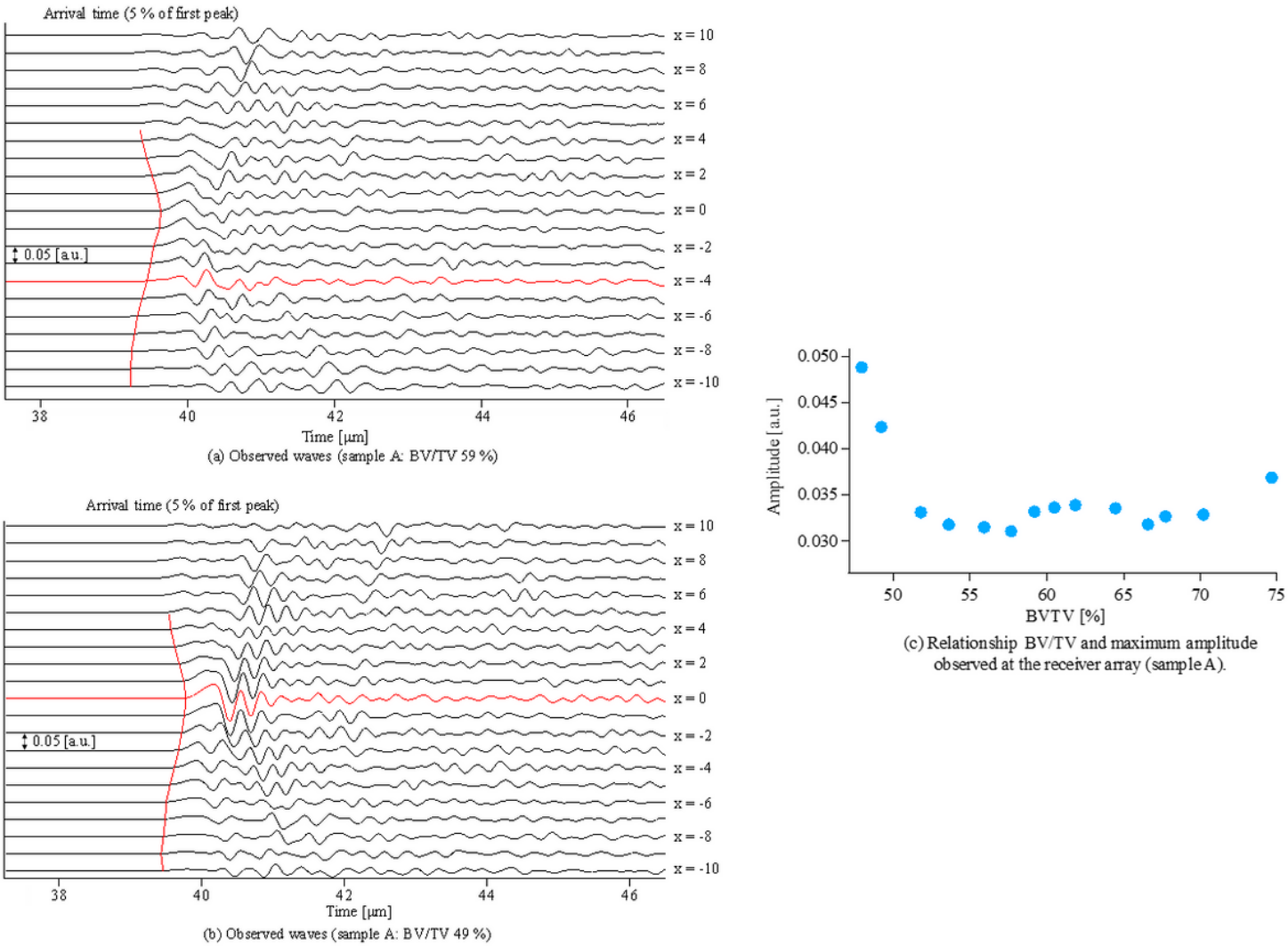

Figure 5

(a) Observed waves which passed through the sample A (BV/TV 59 %), near the center of the receiver array. (b) Observed waves which passed through the sample A (BV/TV 49 %), near the center of the receiver array. (c) Relationship BV/TV and maximum amplitude observed at the receiver array (sample A).

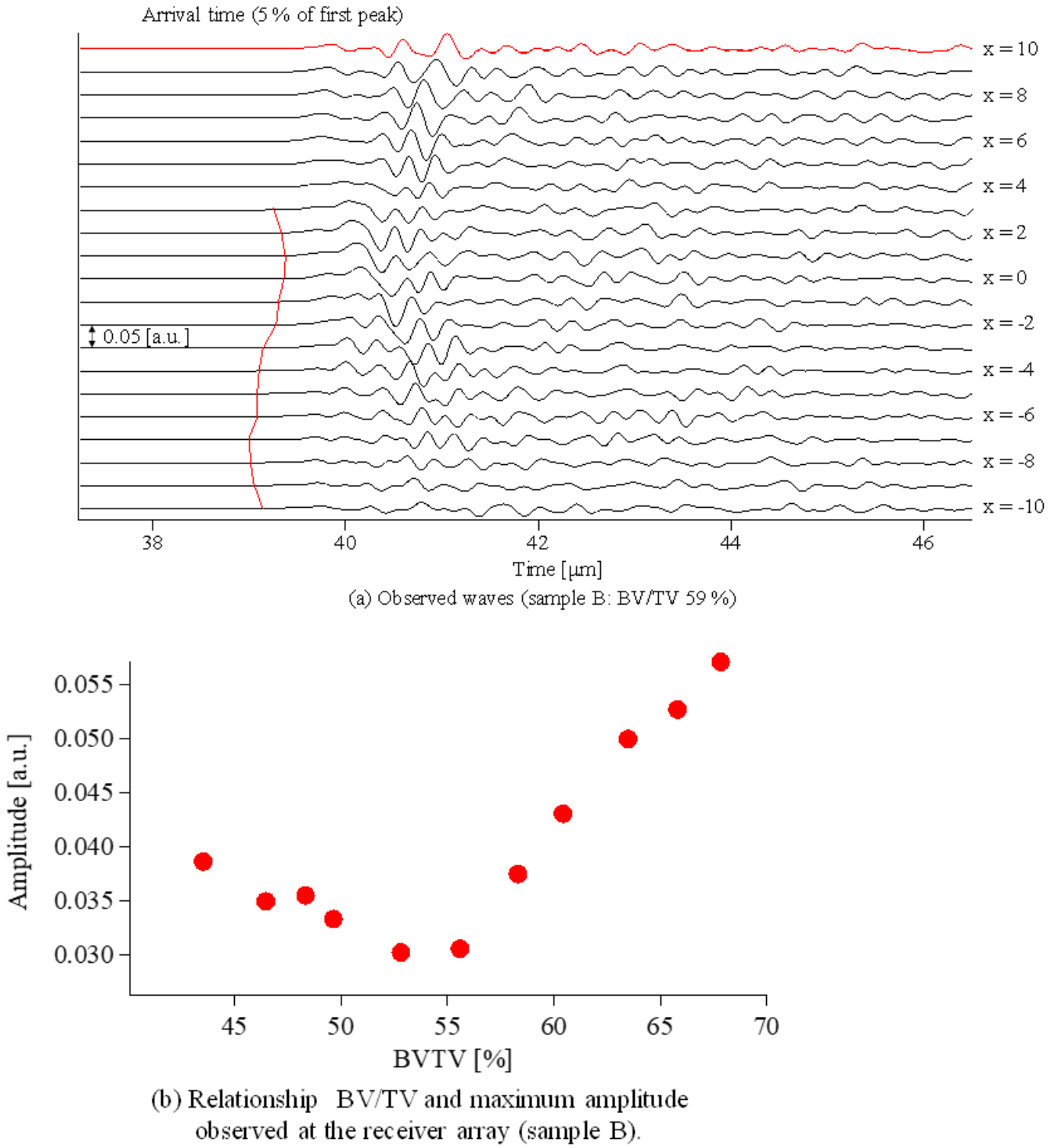

Figure 6

(a) Observed waves which passed through the sample B (BV/TV 59 %) near the center of the receiver array. (b) Relationship BV/TV and maximum amplitude observed at the receiver array (sample B).

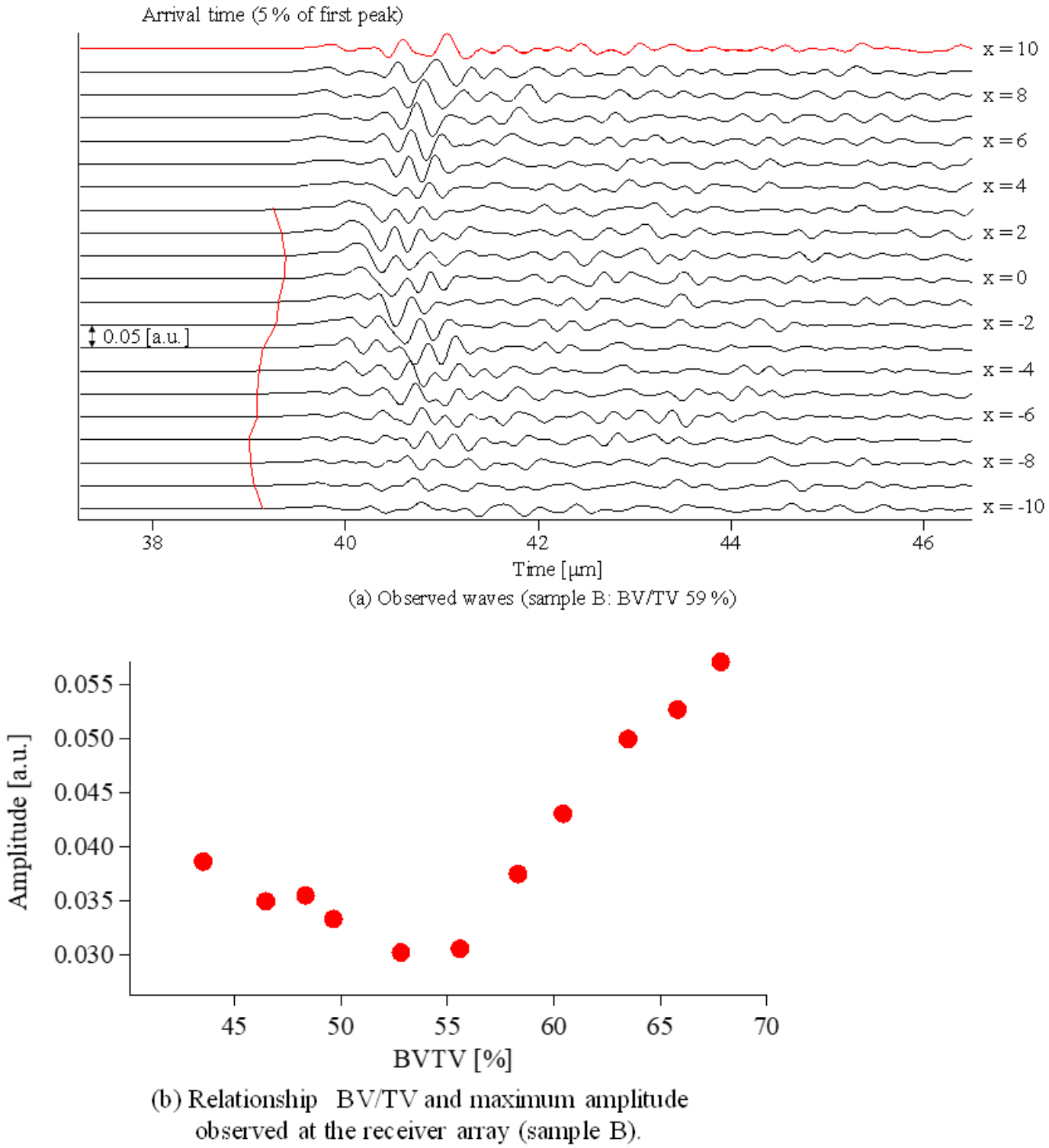

Figure 6

(a) Observed waves which passed through the sample B (BV/TV 59 %) near the center of the receiver array. (b) Relationship BV/TV and maximum amplitude observed at the receiver array (sample B).

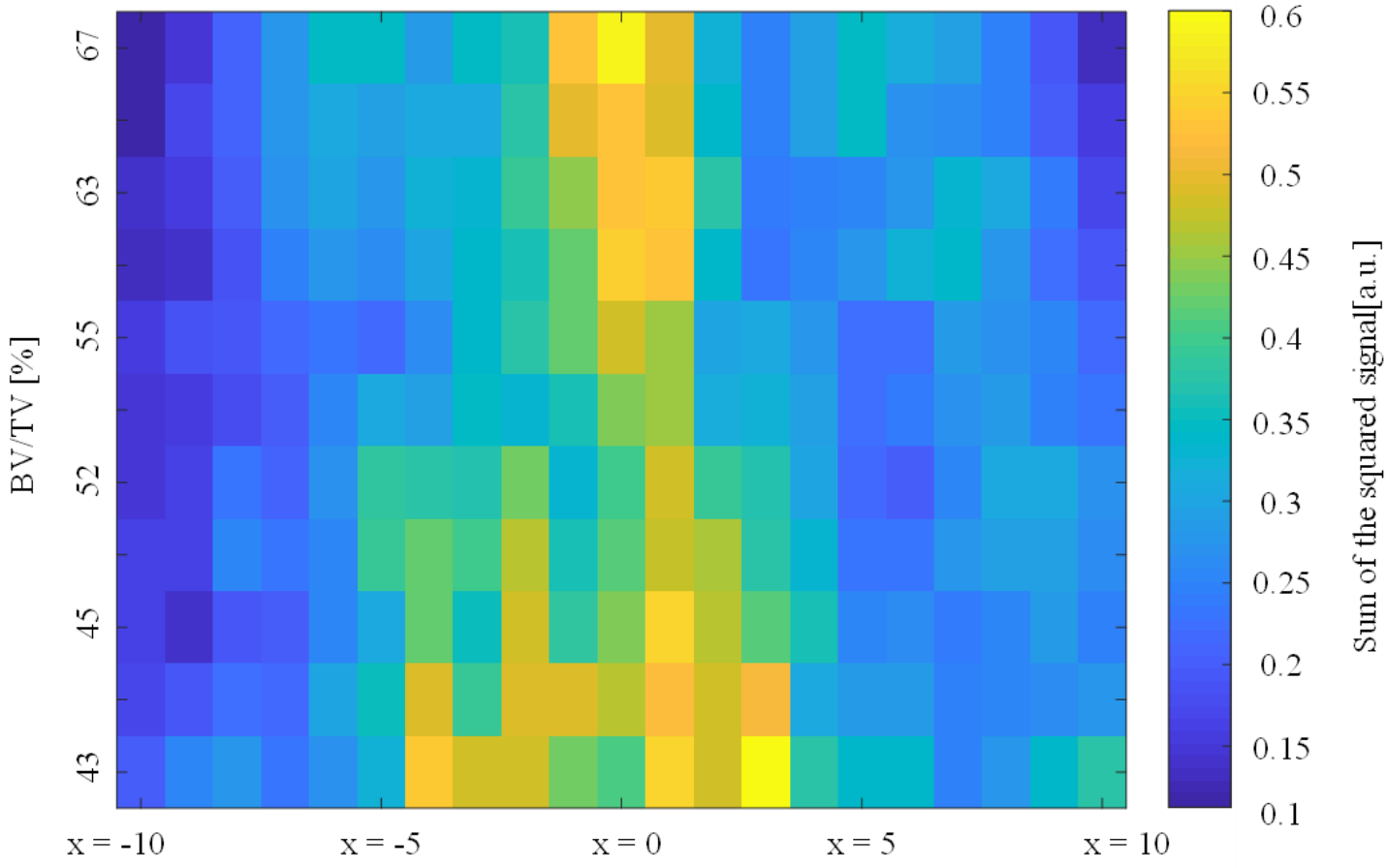

Figure 7

The relationships between sum of the squared signal observed at each receiver as a function of BV/TV (sample B).

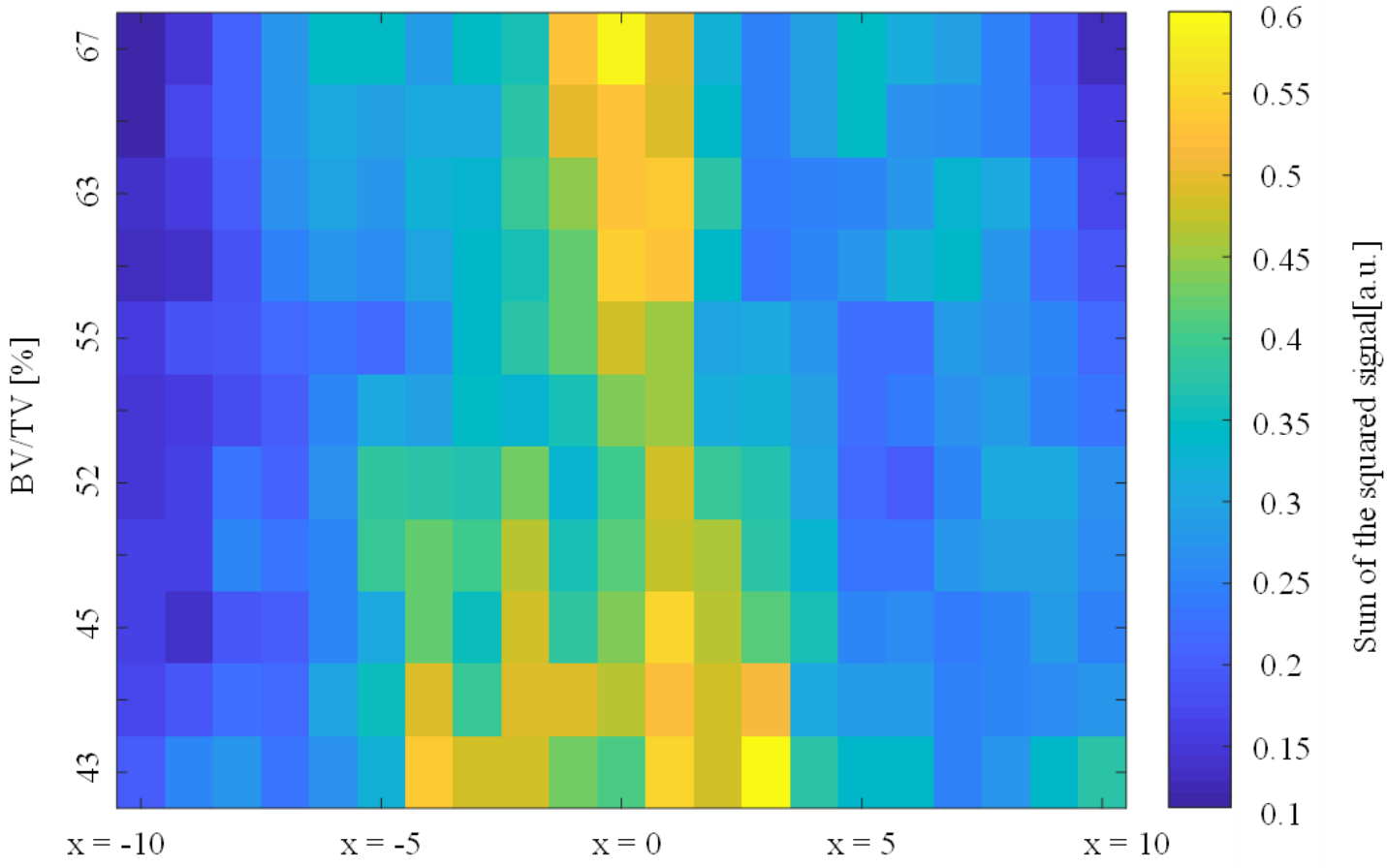

Figure 7

The relationships between sum of the squared signal observed at each receiver as a function of BV/TV (sample B).